Bergische Universität Wuppertal

Fakultät für Mathematik und Naturwissenschaften

Institute of Mathematical Modelling, Analysis and Computational Mathematics (IMACM)

Preprint BUW-IMACM 23/02

Gustavo Morais Rodrigues Costa, Marcelo Lobosco, Matthias Ehrhardt, and Ruy Freitas Reis

Mathematical Analysis and a Nonstandard Scheme for a Model of the Immune Response against COVID-19

January 3, 2023

http://www.imacm.uni-wuppertal.de

Mathematical Analysis and a Nonstandard Scheme for a Model of the Immune Response Against COVID-19

Gustavo Morais Rodrigues Costa, Marcelo Lobosco, Matthias Ehrhardt, and Ruy Freitas Reis

This paper is dedicated in honor of Ronald E. Mickens' 80th birthday.

Abstract. In this work, we consider a compartmental model to describe the immune response to SARS-CoV-2. The model considers the primary cells involved in the body's immune response, antigen-presenting cells, CD4+ and CD8+ T cells, B cells, IgM and IgG antibodies, proinflammatory cytokines, and infected cells of the immune system. The resulting system consists of 15 ordinary differential equations (ODEs) with 38 parameters.

For the numerical solution of this rather large ODE system, we develop a special non-standard finite difference (NSFD) scheme that preserves the positivity of the solutions.

1. Introduction

The first case of the coronavirus disease (COVID-19) was detected in Wuhan, China, in December 2019. The virus rapidly spread, and by February 2020, there were cases of this new disease in 8 countries. Deeply concerned about the alarming spread of the disease, its severity, and the lack of action, the World Health Organization (WHO) declared COVID-19 a global pandemic in March 2020 [**43**].

By December 22, 2022, COVID-19 had already infected more than 655 million people worldwide, 244 million in Europe, 100 million only in the United States of America, and 36 million in Brazil, as shown in Figure 2A. On the other hand, the number of worldwide deaths at the same time was more than 6.67 million, 2 million in Europe, 1.09 million in the United States of America, and 692,652 in Brazil, as shown in Figure 2B. Even after the first dose of vaccine was administered in December 2020 [**31**], more than 3 million people died from COVID-19 infection. Figure 1 illustrates the relationship between the population size of each country, the number of infected people, and the number of deaths.

Even though the pandemic started more than three years ago, there are still open questions regarding COVID-19. Some of these questions can be answered with the help of mathematical models and *in silico* trials. The numerical results obtained

2020 *Mathematics Subject Classification.* Primary 65L05, 92C60.

Key words and phrases. nonstandard finite difference scheme, COVID-19, compartmental models, computational immunology, differential evolution.

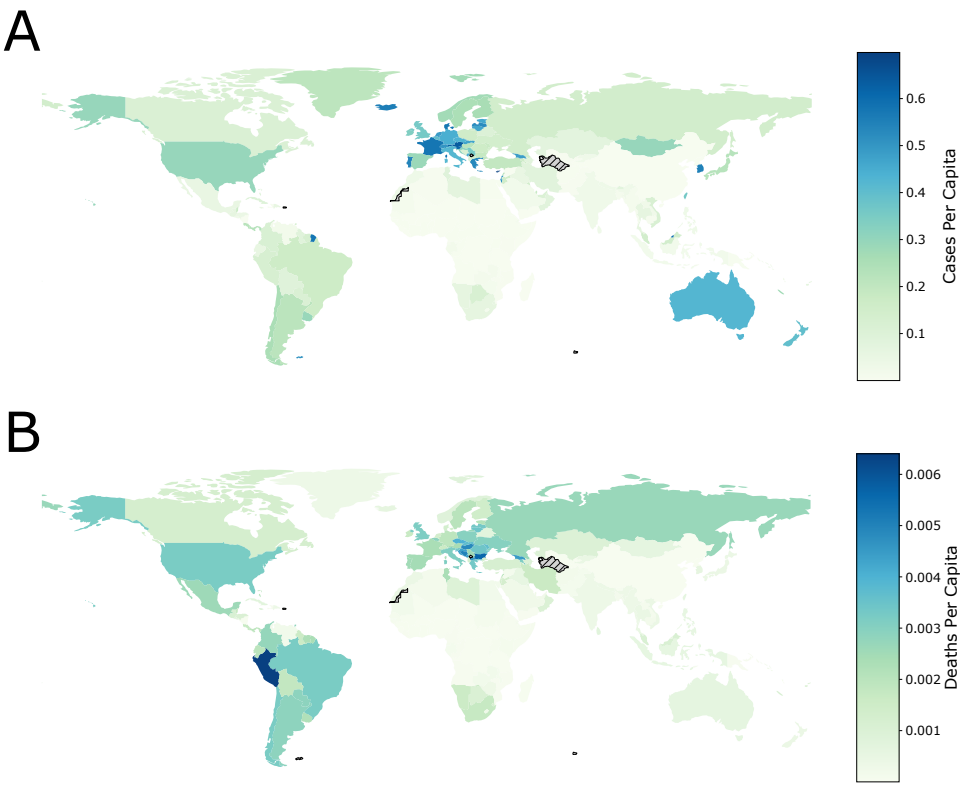

FIGURE 1. Choropleth map showing the incidence of COVID-19 around the globe. Panel A presents the number of COVID-19 cases compared with the total population, while Panel B presents the number of deaths as complications of COVID-19 compared with the total population. Crosshatched black and grey areas identify locations where no data is available.

from these trials might reveal information that may lead the scientific community to understand this disease. A considerable amount of work makes use of mathematical and computational modeling to understand how the *human immune system* (HIS) works by different means, such as ordinary differential equations (ODEs) [**24, 1, 7, 42, 18, 2, 30**], partial differential equations (PDEs) [**25, 40, 13, 27, 10**], and stochastic methods [**8, 44**].

This work uses a mathematical model to represent the immune response against SARS-CoV-2 [**30**]. This model considers the primary cells involved in the body's immune response, antigen-presenting cells, CD4+ and CD8+ T cells, B cells, IgM and IgG antibodies, pro-inflammatory cytokines, and infected immune system cells. The model is composed of 15 ODEs and has 38 parameters. In this work, we adjusted and validated the model using a new set of cohort data [**46**] referring to CD4+ (Effector T Helper Cells), CD8+ (Effector T Killer Cells), and the viremia obtained from COVID-19 patients. *Differential Evolution* (DE) [**39**] was used to adjust the model parameters.

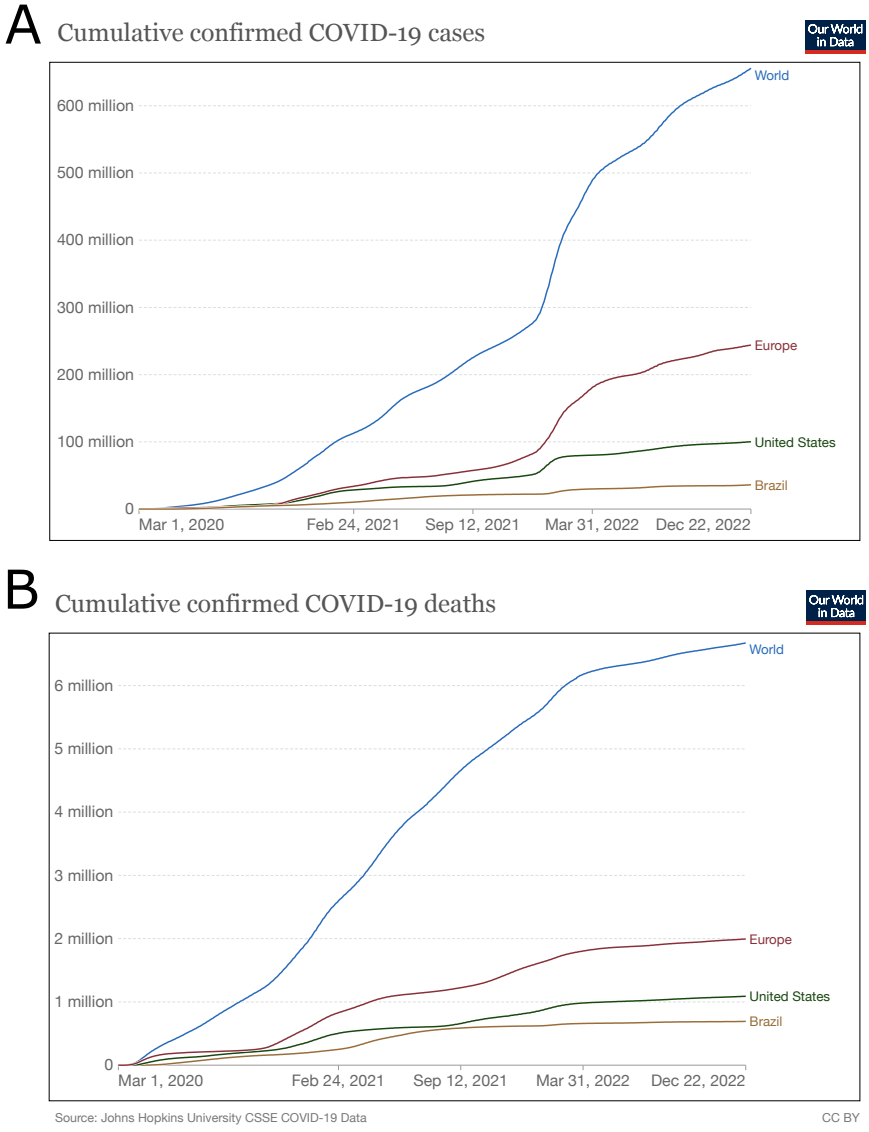

FIGURE 2. Evolution of cumulative confirmed COVID-19 cases (A) and confirmed COVID-19 deaths (B). A) Due to limited testing, the number of confirmed cases is lower than the true number of COVID-19 infections [**31**]. B) Due to varying protocols and challenges in defining the cause of death, the number of confirmed deaths may not accurately represent the true death toll of COVID-19.

Additionally, sensitivity analysis via Sobol main indexes [**37**] made it possible to gather further information on the immune response to SARS-CoV-2. Furthermore, we employ the *Non-Standard Finite Difference* (NSFD) approach to designing a

numerical method specially designed for our system. To the best of our knowledge, this type of numerical scheme has not been used to solve large ODEs systems such as this one. So, this study is interested in demonstrating whether this numerical scheme is able to solve large systems of ODEs.

This work is organized as follows. Section 2 presents a brief introduction to the Immunological System to help achieve a better understanding of the matter at hand. Section 3 presents the mathematical model (3.1), which was solved using the NSFD Scheme presented in Section 3.2, adjusted to the data extracted as in Section 3.3 with the use of DE (Section 3.4), understood with the help of Sensitivity Analysis presented in Section 3.5. Section 4 presents the results obtained from our study, which we delve into further in Section 5. Finally, the last section presents our conclusions and plans for future work.

2. Immunological Background

The *human immune system* (HIS) consists of several mechanisms that work together to ensure the health of the human body. Some of its elements act directly on the immunological response to antigens, such as T-killer cells (CD8+). With the help of antigen-presenting cells (APCs) and cytokines, these cells can recognize and eliminate various threats that enter our bodies, such as viruses and bacteria.

The HIS defense against antigens is made up of two main parts: the innate and the adaptive immune systems. The innate system acts as the first layer of defense against any type of pathogen, while the adaptive system is tailored to deal with specific types of antigens, including viruses. The adaptive defense system can evolve throughout our lives to protect us against almost any invader.

When APCs and other stimuli activate T helper cells, a cascade of events is triggered, leading to the activation of B and T-killer cells. The functions of T-killer cells include identifying and destroying virus-infected cells. A distinct strategy to kill viruses involves the production of antibodies. Antibodies opzonize and prepare viruses to be eliminated by phagocytes. Mature B cells are responsible for specific antibody production. Thus, the receptors on the various B cells are so diverse that our B cells can probably recognize any organic molecule that exists and produce specific antibodies for it. After the infection is under control, some B cells differentiate into memory B cells to maintain information about how to repel future invasions of the same antigen. The necessary amount of memory B cells is stored for this purpose. These memory B cells can be reactivated faster to produce specific antibodies against the same invader.

In this work, we focus on the adaptive immune system, working on a model that describes antigen-presenting cells, the T cells, and some types of antibodies (IgG and IgM) besides the virus and the cytokines. The original model [**3**] was adapted to describe the specific response to coronavirus infection [**30**]. A difference is that this paper includes CD4+ and CD8+ data [**46**] to adjust and analyze the results of the *in silico* experiments. The focus on this population can be explained by the T cells' role in understanding the severity of COVID-19 cases since lymphopenia is an indicator of SARS-CoV-2 infection and a predictive of disease progression.

3. Material and Methods

3.1. Mathematical Model. In this work, we use a model composed of 15 ODE [**30**]s, where each one represents an element involved in the immune system

response to SARS-CoV-2 infection: virus (I); naive (T_{hn}) and effector (T_{he}) T helper (CD4+) cells; naive (T_{kn}) and effector (T_{ke}) T Killer (CD8+) cells; B cells (B); short- (P_s) and long-lived (P_l) plasma cells; B memory cells (B_m); IgM (Ig_M) and IgG (Ig_G) antibodies, and cytokines (C).

The first equation represents SARS-CoV-2 (V) usage of the cell machinery to replicate itself and spread to other cells, as well as its interaction with the immune system [**6, 16, 35**]. The first term of Eq. (3.16a), $\pi_v V$, expresses the replication of the virus since pi_v represents the growth rate of the SARS-CoV-2. The other terms of Eq. (3.16a) indicate the elimination rate of the virus by the immune system. The antibodies can opsonize the virus to facilitate the binding of the virus to receptor molecules present in phagocytes [**23**]. This phenomenon is denoted by the second and the third terms of Eq. (3.16a): the term $k_{v1} V I_{gG}$ illustrates the death of the virus due to its opsonization by I_{gG}, and the term $k_{v1} V I_{gM}$ due to its opsonization by I_{gM}, respectively, being k_{v1} the rate at which an antibody opsonizes a virus. The term $k_{v2} V T_{ke}$, where k_{v2} is the clearance rate, represents viral clearance due to the induction of apoptosis of cells infected by the SARS-CoV-2 virus. Finally, $k_{v3} V A_{pm}$depicts the viral clearance by mature APCs, such as macrophages, where the term k_{v3} is the clearance rate.

$$\frac{d}{dt}V = \pi_v V - k_{v1} V I_{gG} - k_{v1} V I_{gM} - k_{v2} V T_{ke} - k_{v3} V A_{pm}. \tag{3.1}$$

Antigen-presenting cells (APC) are found in two stages, naive and mature [**22**]. The second and third equations represent these two stages of the APCs, naive (A_p) and mature (A_{pm}). APCs are those cells specialized in presenting an antigen to a T-cell. Distinct immune cells can act as APC. In this work, we consider that the main APCs are macrophages. In Eq. (3.2), the naive APCs' homeostasis and activation are described by the first and second terms, respectively. Pro-inflammatory cytokines influence the homeostatic balance of the APCs [**22**], and, for this reason, in the first term, $\alpha_{ap}(C+1)(A_{p0} - A_p)$, α_{ap} represents the homeostasis rate and $(C+1)$ represents the influence of pro-inflammatory cytokines in the homeostasis. The term $\beta_{ap} A_p \frac{c_{ap1} V}{c_{ap2}+V}$ denotes the conversion of immature APCs into mature ones which explains why the same term appears in Eq. (3.3) with a positive sign. Moreover, this last term uses a function to model growth combined with the saturation phenomenon [**14**].

$$\frac{d}{dt}A_p = \alpha_{ap}(C+1)(A_{p0} - A_p) - \beta_{ap} A_p \frac{c_{ap1} V}{c_{ap2} + V}. \tag{3.2}$$

In Eq. (3.3), which represents mature APCs, $\beta_{apm} A_{pm} V$ denotes A_{pm} infection by the SARS-CoV-2 virus, where β_{apm} is the infection rate. In other words, this term considers the hypothesis that SARS-CoV-2 also infects immune cells [**15, 9**], thus causing the production of several pro-inflammatory cytokines (mainly IL-6), which may cause a Cytokine Release Syndrome (CRS) or cytokine storm. The third term, $\delta_{apm} A_{pm}$, means the natural decay of the mature APCs, where δ_{apm} is the decay rate.

$$\frac{d}{dt}A_{pm} = \beta_{ap} A_p \frac{c_{ap1} V}{c_{ap2} + V} - \beta_{apm} A_{pm} V - \delta_{apm} A_{pm}. \tag{3.3}$$

The dynamics of the infected immune system cells are represented by Eq. (3.4). The first term, $\beta_{apm}A_{pm}V$, represents A_{pm} infection, and the second term, $\beta_{tke}T_{ke}V$, represents CD8+ T cell infection. The infection rates are, respectively, β_{apm} and β_{tk}. Infected cells die with a rate δ_{apm}.

$$\frac{d}{dt}I = \beta_{apm}A_{pm}V + \beta_{tke}T_{ke}V - \delta_{apm}I. \tag{3.4}$$

Eq. (3.5) represents the population of naive CD4+ T cells (T_{hn}). The term $\alpha_{th}(T_{hn0} - T_{hn})$ represents the homeostasis of CD4+ T cells, where α_{th} is the homeostasis rate. APCs are responsible for activating naive CD4+ T cells [**22**]. The term $\beta_{th}A_{pm}T_{hn}$ denotes the activation of naive CD4+ T cells, where β_{th} is the activation rate.

$$\frac{d}{dt}T_{hn} = \alpha_{th}(T_{hn0} - T_{hn}) - \beta_{th}A_{pm}T_{hn}. \tag{3.5}$$

Eq. (3.6) represents the effector CD4+ T cell population (T_{he}). The term $\pi_{th}A_{pm}T_{he}$ represents the proliferation of effector CD4+ T cells, where π_{th} is the proliferation rate. The term $\delta_{th}T_{he}$ represents the natural death of these cells, with δ_{th} representing its death rate.

$$\frac{d}{dt}T_{he} = \beta_{th}A_{pm}T_{hn} + \pi_{th}A_{pm}T_{he} - \delta_{th}T_{he}. \tag{3.6}$$

Eqs. (3.7) and (3.8) represent the population of naive (T_{kn}) and effector (T_{ke}) CD8+ T cells, respectively. In Eq. (3.7), the naive CD8+ T cell's homeostasis and activation are described by the first and second terms, respectively. In the first term, $\alpha_{tk}(C+1)(T_{kn0} - T_{kn})$, α_{tk} represents the homeostasis rate. The term $\beta_{tk}(C+1)A_{pm}T_{kn}$ denotes the activation of naive CD8+ T cells, where β_{tk} is the activation rate. As one can see, pro-inflammatory cytokines (C) influence the homeostatic balance and activation of naive CD8+ T cells.

$$\frac{d}{dt}T_{kn} = \alpha_{tk}(C+1)(T_{kn0} - T_{kn}) - \beta_{tk}(C+1)A_{pm}T_{kn}. \tag{3.7}$$

In Eq. (3.8), the term $\pi_{tk}A_{pm}T_{ke}$ represents the proliferation of effector CD8+ T cells. The terms $\beta_{tke}T_{ke}V$ and $\delta_{tk}T_{ke}$ represent the infection and death of effector CD8+ T cells, respectively.

$$\frac{d}{dt}T_{ke} = \beta_{tk}(C+1)A_{pm}T_{kn} + \pi_{tk}A_{pm}T_{ke} - \beta_{tke}T_{ke}V - \delta_{tk}T_{ke}. \tag{3.8}$$

Eq. (3.9) represents both naive and effector B cells (B). These populations were considered together in order to simplify the model. The term $\alpha_b(B_0 - B)$ represents the B cell's homeostasis, where α_b is the homeostasis rate. The terms $\pi_{b1}VB$ and $\pi_{b2}T_{he}B$ represent the proliferation of B cells activated by the T-cell independent and T-cell dependent mechanisms [**38**], respectively. The terms $\beta_{ps}A_{pm}B$, $\beta_{pl}T_{he}B$ and $\beta_{bm}T_{he}B$ denote the differentiation of active B cells into short-lived plasma cells, long-lived plasma cells, and memory B cells, respectively. The activation rates are respectively given by β_{ps}, β_{pl} and β_{bm}.

$$\frac{d}{dt}B = \alpha_b(B_0 - B) + \pi_{b1}VB + \pi_{b2}T_{he}B - \beta_{ps}A_{pm}B - \beta_{pl}T_{he}B - \beta_{bm}T_{he}B. \tag{3.9}$$

The dynamics of memory B Cells (B_m) is depicted by Eq. (3.10). The logistic growth of memory B cells is represented by the term $\pi_{bm1}B_m\left(1 - \frac{B_m}{\pi_{bm2}}\right)$, *i.e.*, there is a limit to this growth [**4**], being π_{bm1} the limits of the growth rate, and pi_{bm2} of the growth per se.

$$\frac{d}{dt}B_m = \beta_{bm}T_{he}B + \pi_{bm1}B_m\left(1 - \frac{B_m}{\pi_{bm2}}\right) - \gamma_{bm}B_m. \tag{3.10}$$

Eq. (3.11) represents the short-lived plasma cells (P_s) [**38**]. The term $\delta_{ps}P_s$ denotes the natural decay of short-lived plasma cells, where δ_{ps} is the decay rate.

$$\frac{d}{dt}P_s = \beta_{ps}A_{pm}B - \delta_{ps}P_s. \tag{3.11}$$

Long-lived plasma cells (P_l) are represented by Eq. (3.12). The second term, $\delta_{pl}P_l$, describes the natural decay of long-lived plasma cells, where δ_{pl} is the decay rate. The term $\gamma_{bm}B_m$ depicts the replenishing of P_l by memory B cells, with γ_{bm} representing the production rate.

$$\frac{d}{dt}P_l = \beta_{pl}T_{he}B - \delta_{pl}P_l + \gamma_{bm}B_m. \tag{3.12}$$

Eqs. (3.13) and (3.14) describe the generation of antibodies. The first term of each equation, $\pi_{ps}P_s$ and $\pi_{pl}P_l$, represent the production of antibodies by their correspondent plasma cells, short-lived and long-lived, respectively. Both π_{ps} and π_{pl} denote the production rates, respectively. The second terms, $\delta_{am}I_{gM}$ and $\delta_{ag}I_{gG}$, describe the natural decay of IgM and IgG antibodies, respectively, with δ_{am} and δ_{ag} representing the decay rate.

$$\frac{d}{dt}I_{gM} = \pi_{ps}P_s - \delta_{am}I_{gM}. \tag{3.13}$$

$$\frac{d}{dt}I_{gG} = \pi_{pl}P_l - \delta_{ag}I_{gG}. \tag{3.14}$$

Finally, the pro-inflammatory cytokine dynamics are described by Eq. (3.15). The first term of this equation, $\pi_{c_{apm}}A_{pm}$, depicts the production of cytokines by A_{pm}, being $\pi_{c_{apm}}$ the rate of production. The next term describes the cytokine production by infected immune cells, with π_{ci} representing the production rate. The term $\pi_{c_{tke}}T_{ke}$ represents the cytokine production by T_{ke} cells, where $\pi_{c_{tke}}$ denotes the production rate. The last term depicts the natural decay of cytokines, with δ_c describing the decay rate.

$$\frac{d}{dt}C = \pi_{c_{apm}}A_{pm} + \pi_{ci}I + \pi_{c_{tke}}T_{ke} - \delta_c C. \tag{3.15}$$

For simplification purposes, the model used in this work [**30**] did not include infected and non-infected epithelial cells, as it would have more constants to adjust and without the availability of data to validate these cell populations over time. The quality of the results, especially those related to the virus population, is unaffected by the use of implicit antigen replication, as previous works have demonstrated [**4, 29, 3, 26**]. It is also assumed that the virus is located in the tissue, where it can infect matured immune cells. The naive cells are activated in the bloodstream (APCs), lymph nodes (CD4 and CD8), or after leaving both [**22, 23, 38**]. It is also assumed that virus is mainly produced by the epithelial tissue, despite some pieces of evidence showing that infected alveolar macrophages can also assist in virus replication [**15**]. The phagocytic activity by infected cells is assumed to be null in this model. The model used in this work considers that infected cells continue the production of pro-inflammatory cytokines. Finally, the model implicitly accounts for the effects of different pro-inflammatory cytokines.

3.2. The Nonstandard Scheme. In addition to properties such as stability and consistency, qualitative properties, such as the preservation of positivity, are also important for biological models like the one described in this work. This is exactly where nonstandard finite difference (NSFD) methods come into play to meet these requirements.

NSFD schemes for the numerical integration of ODEs were pioneered by Mickens [**20**]. This section presents an NSFD method to solve the resulting ODE system presented in Eq. (3.16). These specialized schemes can be regarded as discrete models of the ODE systems. In this direction, they are designed in order to preserve certain properties such as the positivity of the analytic solution of the ODE system. These schemes can be reformulated in an efficient explicit way, and as a byproduct of the positivity preserving property, the NSFD methods are stable.

For ease of presentation, we rewrite the equations described so far in one ODE system, as shown below.

$$\frac{d}{dt}V = \pi_v V - k_{v1} V I_{gG} - k_{v1} V I_{gM} - k_{v2} V T_{ke} - k_{v3} V A_{pm}, \tag{3.16a}$$

$$\frac{d}{dt}A_p = \alpha_{ap}(C+1)(A_{p0} - A_p) - \beta_{ap} A_p \frac{c_{ap1} V}{c_{ap2} + V}, \tag{3.16b}$$

$$\frac{d}{dt}A_{pm} = \beta_{ap} A_p \frac{c_{ap1} V}{c_{ap2} + V} - \beta_{apm} A_{pm} V - \delta_{apm} A_{pm}, \tag{3.16c}$$

$$\frac{d}{dt}I = \beta_{apm} A_{pm} V + \beta_{tke} V T_{ke} - \delta_{apm} I, \tag{3.16d}$$

$$\frac{d}{dt}T_{hn} = \alpha_{th}(T_{hn0} - T_{hn}) - \beta_{th} A_{pm} T_{hn}, \tag{3.16e}$$

$$\frac{d}{dt}T_{he} = \beta_{th} A_{pm} T_{hn} + \pi_{th} A_{pm} T_{he} - \delta_{th} T_{he}, \tag{3.16f}$$

$$\frac{d}{dt}T_{kn} = \alpha_{tk}(C+1)(T_{kn0} - T_{kn}) - \beta_{tk}(C+1) A_{pm} T_{kn}, \tag{3.16g}$$

$$\frac{d}{dt}T_{ke} = \beta_{tk}(C+1) A_{pm} T_{kn} + \pi_{tk} A_{pm} T_{ke} - \beta_{tke} V T_{ke} - \delta_{tk} T_{ke}, \tag{3.16h}$$

$$\frac{d}{dt}B = \alpha_b(B_0 - B) + \pi_{b1} V B + \pi_{b2} T_{he} B - \beta_{ps} A_{pm} B$$

$$- \beta_{pl} T_{he} B - \beta_{bm} T_{he} B, \tag{3.16i}$$

$$\frac{d}{dt} P_s = \beta_{ps} A_{pm} B - \delta_{ps} P_s, \tag{3.16j}$$

$$\frac{d}{dt} B_m = \beta_{bm} T_{he} B + \pi_{bm1} B_m \Big(1 - \frac{B_m}{\pi_{bm2}}\Big) - \gamma_{bm} B_m, \tag{3.16k}$$

$$\frac{d}{dt} P_l = \beta_{pl} T_{he} B - \delta_{pl} P_l + \gamma_{bm} B_m, \tag{3.16l}$$

$$\frac{d}{dt} I_{gM} = \pi_{ps} P_s - \delta_{am} I_{gM}, \tag{3.16m}$$

$$\frac{d}{dt} I_{gG} = \pi_{pl} P_l - \delta_{ag} I_{gG}, \tag{3.16n}$$

$$\frac{d}{dt} C = \pi_{c_{apm}} A_{pm} + \pi_{ci} I + \pi_{c_{tke}} T_{ke} - \delta_c C. \tag{3.16o}$$

One can easily observe that, for positive parameters and positive initial data, the solution of Eq.(3.16) remains positive all the time. We will call this the "positivity property".

NSFD schemes go back to a paper by Mickens published in 1989 [**21**]. Their structural properties come from investigations of special groups of ODEs for which no exact finite difference schemes are available. In contrast to conventional finite difference methods, NSFD schemes consider not only stability and consistency order, but also pay attention to qualitative properties, *i.e.*, how well does the discrete model (the NSFD scheme) model the most important properties of the underlying continuous model?

We introduce a time step $h > 0$ and consider temporal grid points $t_n := nh$, $n = 0, 1, \ldots$. In the sequel, we denote by V^n the approximation of V at the grid point t_n, and similarly for the other components in Eq. (3.16). In NSFD schemes, derivatives have to be modeled by proper discrete analogs, *i.e.* nonstandard difference quotients of the form, cf. [**20**]

$$\frac{\mathrm{d}}{\mathrm{d}t} V(t_n) \to \frac{V^{n+1} - \psi(h) V^n}{\phi(h)}\,, \tag{3.17}$$

where $\psi(h) = 1 + \mathcal{O}(h)$ and the denominator function $\phi(h) = h + \mathcal{O}(h^2)$. Using this rather general time discretization in NSFD schemes, our aim is to preserve the positivity of the solution, which is the most important structural property. We choose here $\psi(h) = 1$ and $\phi(h) = h$ and focus on the discretization of the right-hand side of the ODE system given by Eq. (3.16).

In an NSFD scheme, the nonlinear terms are approximated in a non-local way, *e.g.* by a suitable function of several grid points, like $V^2(t_n) \approx V^n V^{n+1}$ or $V^3(t_n) \approx (V^n)^2 V^{n+1}$. First, we write down the nonstandard discretization of the 15 components of the ODE system:

$$\frac{V^{n+1} - V^n}{\Phi(h)} = \Pi_v V^{n+1} - k_{v1} I_{gG}^n V^{n+1} - k_{v1} I_{gM}^n V^{n+1} - k_{v2} T_{ke}^n V^{n+1}$$
$$- k_{v3} A_{pm}^n V^{n+1}, \tag{3.18a}$$

$$\frac{A_p^{n+1} - A_p^n}{\Phi(h)} = \alpha_{ap}(C+1)\big(A_{p0} - A_p^{n+1}\big) - \beta_{ap} \frac{c_{ap1} V^{n+1}}{c_{ap2} + V^{n+1}} A_p^{n+1}, \tag{3.18b}$$

$$\frac{A_{pm}^{n+1}-A_{pm}^{n}}{\Phi(h)} = \beta_{ap}\frac{c_{ap1}V^{n+1}}{c_{ap2}+V^{n+1}}A_{p}^{n+1} - \beta_{apm}V^{n+1}A_{pm}^{n+1} - \delta_{apm}A_{pm}^{n+1}, \tag{3.18c}$$

$$\frac{I^{n+1}-I^{n}}{\Phi(h)} = \beta_{apm}A_{pm}^{n+1}V^{n+1} + \beta_{tke}T_{ke}^{n}V^{n+1} - \delta_{apm}I^{n+1}, \tag{3.18d}$$

$$\frac{T_{hn}^{n+1}-T_{hn}^{n}}{\Phi(h)} = \alpha_{th}(T_{hn0}-T_{hn}^{n+1}) - \beta_{th}A_{pm}^{n+1}T_{hn}^{n+1}, \tag{3.18e}$$

$$\frac{T_{he}^{n+1}-T_{he}^{n}}{\Phi(h)} = \beta_{th}A_{pm}^{n+1}T_{hn}^{n+1} + \Pi_{th}A_{pm}^{n+1}T_{he}^{n+1} - \delta_{th}T_{he}^{n+1}, \tag{3.18f}$$

$$\frac{T_{kn}^{n+1}-T_{kn}^{n}}{\Phi(h)} = \alpha_{tk}(C+1)\big(T_{kn0}-T_{kn}^{n+1}\big) - \beta_{tk}(C+1)A_{pm}^{n+1}T_{kn}^{n+1}, \tag{3.18g}$$

$$\begin{aligned}\frac{T_{ke}^{n+1}-T_{ke}^{n}}{\Phi(h)} &= \beta_{tk}A_{pm}^{n+1}T_{kn}^{n+1} + \Pi_{tk}A_{pm}^{n+1}T_{ke}^{n+1} - \beta_{tke}V^{n+1}T_{ke}^{n+1}\\ &\quad - \delta_{tk}T_{ke}^{n+1},\end{aligned} \tag{3.18h}$$

$$\begin{aligned}\frac{B^{n+1}-B^{n}}{\Phi(h)} &= \alpha_{b}(B_{0}-B^{n+1}) + \Pi_{b1}V^{n+1}B^{n+1} + \Pi_{b2}T_{he}^{n+1}B^{n+1}\\ &\quad - \beta_{ps}A_{pm}^{n+1}B^{n+1} - \beta_{pl}T_{he}^{n+1}B^{n+1} - \beta_{pm}T_{he}^{n+1}B^{n+1},\end{aligned} \tag{3.18i}$$

$$\frac{P_{s}^{n+1}-P_{s}^{n}}{\Phi(h)} = \beta_{ps}A_{pm}^{n+1}B^{n+1} - \delta_{ps}P_{s}^{n+1}, \tag{3.18j}$$

$$\frac{B_{m}^{n+1}-B_{m}^{n}}{\Phi(h)} = \beta_{bm}T_{he}^{n+1}B^{n+1} + \Pi_{bm1}B_{m}^{n+1}\Big(1-\frac{B_{m}^{n}}{\Pi_{bm2}}\Big) - \gamma_{bm}B_{m}^{n+1}, \tag{3.18k}$$

$$\frac{P_{l}^{n+1}-P_{l}^{n}}{\Phi(h)} = \beta_{pe}T_{he}^{n+1}B^{n+1} - \delta_{pl}P_{l}^{n+1} + \gamma_{bm}B_{m}^{n+1}, \tag{3.18l}$$

$$\frac{I_{gM}^{n+1}-I_{gM}^{n}}{\Phi(h)} = \Pi_{ps}P_{s}^{n+1} - \delta_{am}I_{gM}^{n+1}, \tag{3.18m}$$

$$\frac{I_{gG}^{n+1}-I_{gG}^{n}}{\Phi(h)} = \Pi_{pl}P_{l}^{n+1} - \delta_{ag}I_{gG}^{n+1}, \tag{3.18n}$$

$$\frac{C^{n+1}-C^{n}}{\Phi(h)} = \Pi_{c_{apm}}A_{pm}^{n+1} + \Pi_{ci}I^{n+1} + \Pi_{c_{tke}}T_{ke}^{n+1} - \delta_{c}C^{n+1}, \tag{3.18o}$$

for $n = 0, 1, \ldots$ and a denominator function $\phi(h) = h$. We briefly comment on the chosen discretizations of the nonlinear terms. For example, in the first line of Eq. (3.18), we have discretized the quadratic term $A_{pm}(t)V(t)$ by $A_{pm}^{n}V^{n+1}$ rather than, say, $A_{pm}^{n}V^{n}$ or $A_{pm}^{n+1}V^{n+1}$. The rule is that exactly one factor of the variable appearing in the time derivative (here V) must be taken at the new time level $n+1$. This is needed to obtain the positivity-preserving property. In order to not destroy the explicit sequential evaluation, all other variables are taken from the previous time level, unless they are already known from a previous step, like $V^{n+1}A_{pm}^{n+1}$ in the third line of Eq. (3.18).

While the NSFD discretization presented in Eq. (3.18) of the ODE system defined in Eq. (3.16) is formally implicit, it can be easily rearranged to obtain a scheme that can be evaluated sequentially in an explicit and thus efficient way:

$$V^{n+1} = \frac{V^{n}}{1+\Phi(h)\big[k_{v1}I_{gG}^{n} + k_{v1}I_{gM}^{n} + k_{v2}T_{ke}^{n} + k_{v3}A_{pm}^{n} - \Pi_{v}\big]}, \tag{3.19a}$$

$$A_p^{n+1} = \frac{A_p^n + \Phi(h)\alpha_{ap}(C+1)A_{p0}}{1+\Phi(h)\left[\alpha_{ap}(C+1) + \beta_{ap}\frac{c_{ap1}V^{n+1}}{c_{ap2}+V^{n+1}}\right]}, \tag{3.19b}$$

$$A_{pm}^{n+1} = \frac{A_{pm}^n + \Phi(h)\beta_{ap}\frac{c_{ap1}V^{n+1}}{c_{ap2}+V^{n+1}}A_p^{n+1}}{1+\Phi(h)\left[\beta_{apm}V^{n+1} + \delta_{apm}\right]}, \tag{3.19c}$$

$$I^{n+1} = \frac{I^n + \Phi(h)\left[\beta_{apm}A_{pm}^{n+1} + \beta_{tke}T_{ke}^n\right]V^{n+1}}{1+\Phi(h)\delta_{apm}}, \tag{3.19d}$$

$$T_{hn}^{n+1} = \frac{T_{hn}^n + \Phi(h)\alpha_{th}T_{hn0}}{1+\Phi(h)\left[\alpha_{th} + \beta_{th}A_{pm}^{n+1}\right]}, \tag{3.19e}$$

$$T_{he}^{n+1} = \frac{T_{he}^n + \Phi(h)\beta_{th}A_{pm}^{n+1}T_{hn}^{n+1}}{1+\Phi(h)\left[\delta_{th} - \Pi_{th}A_{pm}^{n+1}\right]}, \tag{3.19f}$$

$$T_{kn}^{n+1} = \frac{T_{kn}^n + \Phi(h)\alpha_{tk}(C+1)T_{kn0}}{1+\Phi(h)(C+1)\left[\alpha_{tk} + \beta_{tk}A_{pm}^{n+1}\right]}, \tag{3.19g}$$

$$T_{ke}^{n+1} = \frac{T_{ke}^n + \Phi(h)\beta_{tk}A_{pm}^{n+1}T_{kn}^{n+1}}{1+\Phi(h)\left[\delta_{tk} + \beta_{tke}V^{n+1} - \Pi_{tk}A_{pm}^{n+1}\right]}, \tag{3.19h}$$

$$B^{n+1} = \frac{B^n + \Phi(h)\alpha_b B_0}{1+\Phi(h)\left[\alpha_b - \Pi_{b1}V^{n+1} + \beta_{ps}A_{pm}^{n+1} + (\beta_{pl}+\beta_{pm}-\Pi_{b2})T_{he}^{n+1}\right]}, \tag{3.19i}$$

$$P_s^{n+1} = \frac{P_s^n + \Phi(h)\beta_{ps}A_{pm}^{n+1}B^{n+1}}{1+\Phi(h)\delta_{ps}}, \tag{3.19j}$$

$$B_m^{n+1} = \frac{B_m^n + \Phi(h)\beta_{bm}T_{he}^{n+1}B^{n+1}}{1+\Phi(h)\left[\gamma_{bm} - \Pi_{bm1}\left(1-\frac{B_m^n}{\Pi_{bm2}}\right)\right]}, \tag{3.19k}$$

$$P_l^{n+1} = \frac{P_l^n + \Phi(h)\left[\beta_{pe}T_{he}^{n+1}B^{n+1} + \gamma_{bm}B_m^{n+1}\right]}{1+\Phi(h)\delta_{pl}}, \tag{3.19l}$$

$$I_{gM}^{n+1} = \frac{I_{gM}^n + \Phi(h)\Pi_{ps}P_s^{n+1}}{1+\Phi(h)\delta_{am}}, \tag{3.19m}$$

$$I_{gG}^{n+1} = \frac{I_{gG}^n + \Phi(h)\Pi_{pl}P_l^{n+1}}{1+\Phi(h)\delta_{ag}}, \tag{3.19n}$$

$$C^{n+1} = \frac{C^n + \Phi(h)\left[\Pi_{c_{apm}}A_{pm}^{n+1} + \Pi_{ci}I^{n+1} + \Pi_{c_{tke}}T_{ke}^{n+1}\right]}{1+\Phi(h)\delta_c}, \tag{3.19o}$$

for $n = 0, 1, \ldots$

The NSFD scheme presented in Eq. (3.19) is *positivity-preserving*, *i.e.*, it always produces non-negative solutions for positive data if the step size h is sufficiently small since all parameters and the denominator function are non-negative. Thus, negative values for the solution are avoided, and as a byproduct, stability with respect to the maximum norm is guaranteed, cf. [**11**].

For an application example where exactly this problem occurs and the numerical solution of the standard solver becomes negative, we refer the reader to the literature [**19**].

3.3. Data Extraction. Studies available in the scientific literature on individuals infected with SARS-CoV-2 were used to evaluate the mathematical model and its numerical implementation with the NSFD scheme. In our case, viremia and

CD4+ and CD8+ levels of patients who survived or died due to COVID-19 were manually extracted from the graphs on CD4+ (T_{he}) and CD8+ (T_{ke}) in Figures 2-b and 2-c of Zhang *et al.* [**46**] and the viral load of Sars-CoV-2 from Figure 2 of To *et al.* [**41**]. This manual process was supported by a tool hosted on `WebPlotDigitizer` website [**32**]. After uploading a target figure to the website, the tool requires some settings regarding axis positions and scale. Then, the desired point data on the figure can be selected to convert it into raw data. The result is a CSV file with comma-separated values containing the x- and y-axis values of each assigned point.

Once we have a coarse grid of extracted point data, we use a first-degree Lagrange interpolation polynomial to approximate the intermediate values [**5**].

3.4. Differential Evolution. *Differential Evolution* (DE) is a stochastic heuristic algorithm that is considered a robust strategy for global optimization [**28**]. The algorithm is inspired by natural evolution in that it features generations, selections, and mutations to better represent an individual's ability to survive in an environment. DE is thus an evolutionary algorithm and a parallel direct search method. It works in generations and represents a population with a given number of individuals, using vectors of parameters to represent each generation. In addition, each vector has a corresponding mutation rate that takes into account the synonym phenomenon occurring in nature, where some positions of the vector are generated randomly. In this way, the offspring of the population is always composed of individuals resulting from the cross between two other individuals of the previous population, also taking into account any mutation that might occur in one of the new individuals. The generation of the offspring continues until convergence, or the maximum number of iterations is reached.

In this work, we attempted to minimize the error between the CD4+, CD8+, and viremia model solution and the corresponding values from the extracted cohort data. To measure the difference between the cohort (λ) and the approximated data ($\hat{\lambda}$), we use the relative error (R_E), as follows:

$$R_E = \frac{||\lambda - \hat{\lambda}||_2}{||\hat{\lambda}||_2}. \tag{3.20}$$

To achieve the parameter estimation with DE, we use an objective function. Thus, in this work, the difference between the model results and the cohort data was minimized using the equation that takes into account not only the relative error between the approximated values of virus (V), CD4+(T_{he}) and CD8+(T_{ke}) but also the weight attributed to w_1, w_2 and w_3, respectively. DE thus performs a search for the values of the p parameters that better fit the curves considering the following objective function:

$$\min_p \big(w_1 R_E(V, \hat{V}) + w_2 R_E(T_{he}, \hat{T}_{he}) + w_3 R_E(T_{ke}, \hat{T}_{ke})\big). \tag{3.21}$$

During our study, the algorithm was improved with the results of each run, and adjusting the weight of each relative error in the objective function was a crucial factor in obtaining the best results. In the end, we found that $w_1 = 1$, $w_2 = 1$, and $w_3 = 2$ were the proper values for matching the model results with the cohort data.

3.5. Sensitivity Analysis. One method of quantifying the influence of parameters in the model is to perform what is called a *sensitivity analysis* [**17**]. Once applying DE to 38 parameters in a set of 15 ordinary differential equations is no

longer practical, we use Sobol main indices to understand which parameters have a greater impact on the equation we are trying to fit and include them in the optimization process performed via DE [**36, 37**].

The method of Sobol main indices requires as input a statistical distribution of each of the parameters to be analyzed. The result of the method indicates the influence of each parameter in the selected time point, ranging from 0 (lowest value) to 1 (highest value). Moreover, once the influence of each parameter has been evaluated relatively, the sum of all parameter indices in the selected time point is equal to 1. Thus, this type of analysis can be used to quantify the influence of an uncertain input p_i on the model.

Considering a general model and its parameters:

$$G = f(p_1, \ldots, p_n), \tag{3.22}$$

where the output G is a scalar and the input or parameters are independent variables that are also randomized and described by *probability density function* (PDF) distributions since they represent the uncertainty of the system. The main idea is to decompose the variation to relate it to the contribution of each parameter.

To perform the sensitivity analysis, we use the parameters as uniform PDF distributions in the range of $[0.6p_i, 1.4p_i]$ for the CD4+ population and $[0.01p_i, 100p_i]$ for CD8+. Thus, we evaluate the influence of a particular p_i parameter at a particular moment of the model solution compared to the others.

4. Results

This section presents the results of the COVID-19 model used, which was fitted to viremia data of SARS-CoV-2, CD4+ (effector T helper cells), and CD8+ (effector T killer cells) in patients with COVID-19.

4.1. Software Specifications. The fitting was done by minimizing the error between the cohort data and numerical results using the DE method. The method `differential_evolution` [**33**] from the `scipy` [**34**] package was used to perform the DE method. In addition, sensitivity analysis using the Sobol index method provides the quantitative influence of the parameters on the model results, which is valuable information for model fitting. The Sobol analysis was performed using the Chaospy tool [**12**]. All simulations were performed using Python 3.9.1. The initial conditions of each population are presented in Tab. 1, while the values if the parameters used to solve the system of ODEs are presented in Tab. 2.

4.2. Influence of parameters in the model. Figure 3 presents the results of the Sobol main indices for both effector T helper and T killer cells. Figure 3A shows that for the population of effector helper T cells, the parameters that had the greatest impact on the simulation result of CD4+ cells were c_{ap1}, β_{tk}, β_{tke}, δ_{apm}, α_{th} and π_{tk}. Figure 3B shows that c_{ap2}, δ_{apm}, β_{ap}, π_v, β_{tk} have a smaller influence on the simulation result of CD8+ cells. Considering this information, most of these parameters are included in the DE variables, where c_{ap1} and β_{tke} belong to the parameters that enter a wider range of the search space (bounds) input for DE.

4.3. Model Adjustment. As shown in Figure 4A, the response to COVID-19 infection in patients with severe cases causes a decline in CD4+ around day 30. After a few days of growth, the CD4+ population begins to decline and halves within approximately 10 days. The model results were able to qualitatively capture

Pop	Value	Unit
A_p	10^6	(cells/mL)
A_{pm}	0	(cells/mL)
I	0	(cells/mL)
T_{hn}	10^6	(cells/mL)
T_{he}	0	(cells/mL)
T_{ke}	500.0×10^3	(cells/mL)
B	0	(cells/mL)
P_s	250.0×10^3	(cells/mL)
P_l	0	(cells/mL)
B_m	0	(cells/mL)
I_{gG}	0	S/CO
I_{gM}	0	S/CO
C	0	(pg/mL)

TABLE 1. The initial values of each population.

this behavior. Furthermore, when the standard deviation of the cohort data is considered, the model results fit within the range of the overall simulation.

Figure 4B shows the model results together with cohort data from the CD8+ population in severe cases of COVID-19. The data show a stable state after 40 days of COVID-19 infection. Similar to the cohort data, the fitted model results show qualitatively the same behavior. We can highlight that the CD8+ emerges after decay, but when we consider the standard deviation of the cohort data, the model results fit within the range of the whole simulation.

5. Discussion

As can be seen in Figure 4, the obtained results show that the curves are qualitatively similar and correspond to the standard deviation of the cohort data.

The insights derived from the sensitivity analysis results guide the fitting of the model in the right direction once the application of DE to so many variables (38 parameters) is ineffective in a large system of ODEs. Performing the Sobol index method followed by DE could provide us with valuable information on whether the parameters should be included in DE. Moreover, each population (CD4+ and CD8+) has its own set of parameters affecting its curves, which explains the different sets of parameters used in each of the Sobol index results shown in Figure 3.

The behavior of CD4+ and CD8+ cells is similar to the cohort data (see 4), whereas their population decreases after the first symptoms of COVID-19. This behavior is justified in the scientific literature when one of the features of SARS-CoV-2 infection is a decreased number of white cells in the blood or lymphocytopenia, which is seen in both the simulation and cohort data.

Moreover, the model results presented in this study were obtained by solving the COVID-19 model using a newly developed NSFD scheme, which favors our hypothesis regarding the convergence of the method, apart from the considerable number of equations in the ODE system.

Parameter	Value	Unit
π_v	6.3482×10^{-1}	(day^{-1})
k_{v1}	0.0098	$(\text{day}^{-1}(\text{mlU/ml})^{-1})$
k_{v2}	2.8469×10^{-5}	$(\text{day}^{-1}(\text{cells/mL})^{-1})$
k_{v3}	0.06452	$(\text{day}^{-1}(\text{cells/mL})^{-1})$
α_{ap}	1	$(\text{day}^{-1}(\text{pg/mL})^{-1})$
β_{ap}	$3.8486x10^{-1}$	$(\text{day}^{-1}(\text{copies/mL})^{-1})$
c_{ap1}	2.4393×10^{5}	(copies/mL)
c_{ap2}	1.1730×10^{12}	(copies/mL)
δ_{apm}	7.0824×10^{-02}	(day^{-1})
β_{apm}	1.9534×10^{-02}	$(\text{day}^{-1}(\text{copies/mL})^{-1})$
β_{tke}	2.2884×10^{-05}	$(\text{day}^{-1}(\text{copies/mL})^{-1})$
α_{th}	1.629510^{-04}	(day^{-1})
β_{th}	1.7124×10^{-05}	$(\text{day}^{-1}(\text{cells/mL})^{-1})$
π_{th}	10^{-8}	$(\text{day}^{-1}(\text{cells/mL})^{-1})$
δ_{th}	1.0518×10^{-01}	(day^{-1})
α_{tk}	1	$(\text{day}^{-1}(\text{pg/mL})^{-1})$
β_{tk}	1.3354×10^{-05}	$(\text{day}^{-1}(\text{pg/mL})^{-1}(\text{cell/mL})^{-1})$
π_{tk}	10^{-8}	$(\text{day}^{-1}(\text{cells/mL})^{-1})$
δ_{tk}	5.6691×10^{-02}	(day^{-1})
α_b	3.5782	(day^{-1})
π_{b1}	8.98×10^{-5}	$(\text{day}^{-1}(\text{copies/mL})^{-1})$
π_{b2}	1.27×10^{-8}	$(\text{day}^{-1}(\text{cells/mL})^{-1})$
β_{ps}	6.00×10^{-6}	$(\text{day}^{-1}(\text{cells/mL})^{-1})$
β_{pl}	5.00×10^{-6}	$(\text{day}^{-1}(\text{cells/mL})^{-1})$
β_{bm}	1.00×10^{-6}	$(\text{day}^{-1}(\text{cells/mL})^{-1})$
δ_{ps}	2.5	(day^{-1})
δ_{pl}	0.35	(day^{-1})
γ_{bm}	0.0009	(day^{-1})
π_{bm1}	1.00×10^{5}	(day^{-1})
π_{bm2}	2500.00	(cells/mL)
π_{ps}	0.087	$(\text{day}^{-1}(\text{cells/mL})^{-1}(\text{S/CO}))$
π_{pl}	0.001	$(\text{day}^{-1}(\text{cells/mL})^{-1}(\text{S/CO}))$
δ_{am}	0.07	(day^{-1})
δ_{ag}	0.07	(day^{-1})
π_{capm}	328.0626434	$(\text{day}^{-1}(\text{pg/mL})(\text{cell/mL})^{-1})$
π_{ci}	0.0064	$(\text{day}^{-1}(\text{pg/mL})(\text{cell/mL})^{-1})$
π_{ctke}	0.01783	$(\text{day}^{-1}(\text{pg/mL})(\text{cell/mL})^{-1})$
δ_c	704.2259	(cells/mL)
V	1.7662×10^{2}	(day^{-1})

TABLE 2. The values of the parameters used to solve the system.

6. Conclusions and Future Work

The results obtained in this study show that the mathematical model used in the numerical experiments is suitable to capture cohort data on CD4+, CD8+,

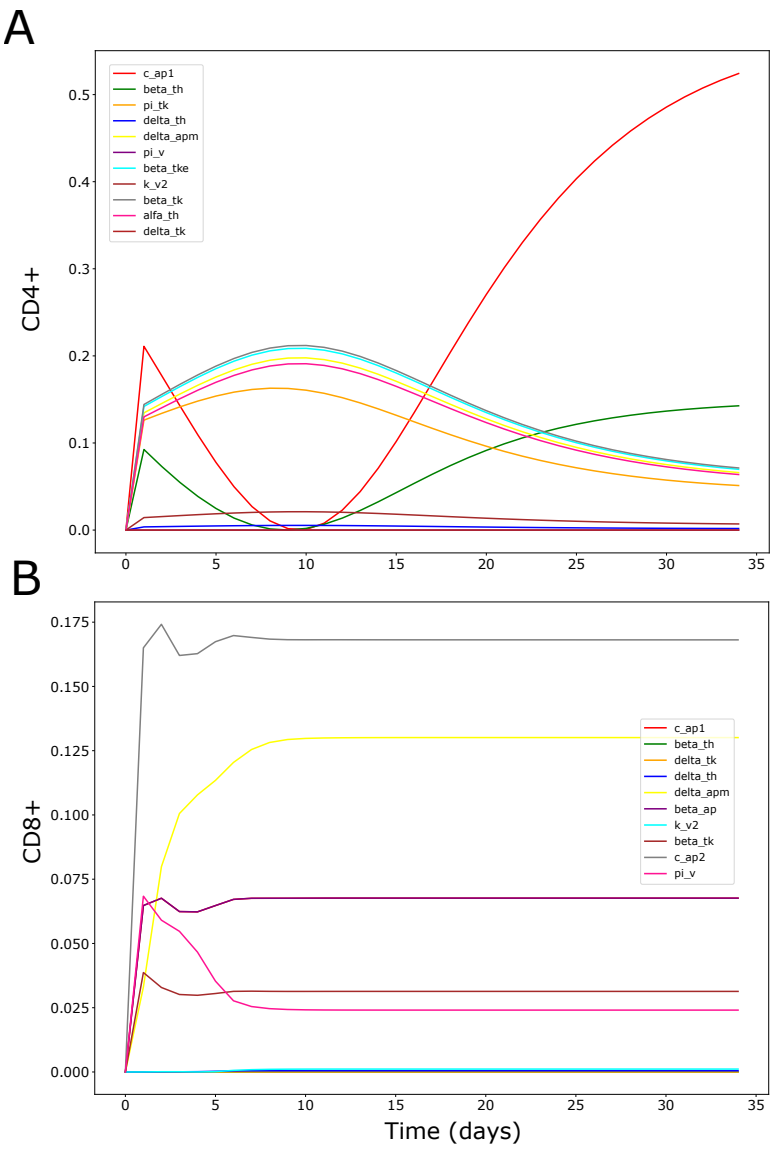

FIGURE 3. The curves in this figure illustrate the influence of each parameter included in the sensitivity analysis on the CD4+ and CD8+ populations. The vertical axis shows the relative influence of each variable on the analysis versus the influence of all included parameters on the Sobol index method. The horizontal axis represents the simulation time such that the overall picture shows the relative influence of each parameter at each time step over 35 days of SARS-CoV-2 infection.

and viremia behavior in severe cases of COVID-19. Moreover, to our knowledge, no NSFD scheme has ever been proposed for such a large ODE system with 15

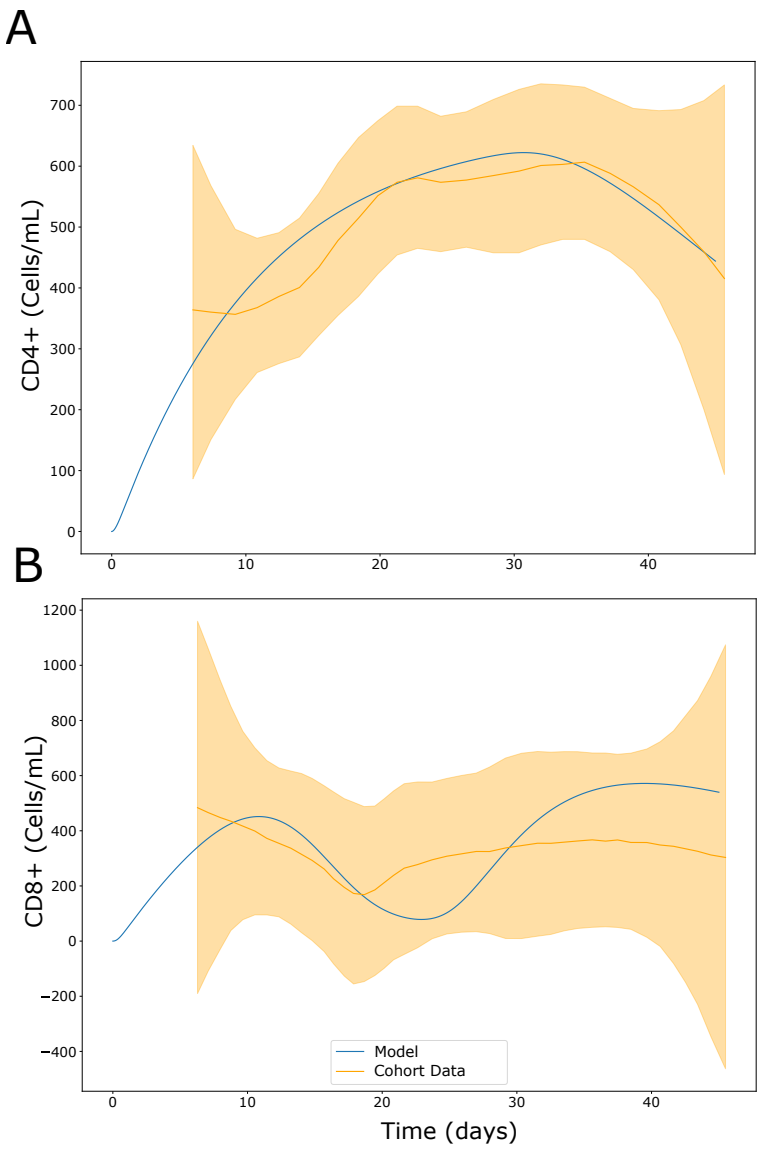

FIGURE 4. The numerical result presented in this figure shows the time variations of the concentrations of CD4+ and CD8+ cells, A and B, respectively. The solution curve, referred to as the "Model" shows the result of solving the ODE system, while the "Cohort Data" curve represents the values obtained from the literature [**45**]. The values of the parameters used to solve the system are given in Table 2, and the initial values can be found in Table 1.

components and 38 parameters. Thus, this work presents evidence for using NFSD schemes for a large system of equations.

Future work will investigate the robustness of this model for various HIS cells that play key roles in SARS-CoV-2 infections.

Acknowledgment

This work has been supported by Universidade Federal de Juiz de Fora (UFJF) through the scholarship BIC/UFJF; by Conselho Nacional de Desenvolvimento Científico e Tecnológico (CNPq) - Brazil grant number 308745/2021-3 and 423278/2021-5; by Fundação de Amparo à Pesquisa do Estado de Minas Gerais (FAPEMIG) - Brazil CEX APQ 02830/17, APQ-01226-21, and APQ-02513-22.

References

[1] C.T.H. Baker, G.A Bocharov, and C.A.H. Paul. Mathematical modelling of the interleukin-2 T-cell system: a comparative study of approaches based on ordinary and delay differential equation. *Comput. Math. Meth. Med.*, 1(2):117–128, 1997.

[2] C.R.B. Bonin, R.W. dos Santos, G.C. Fernandes, and M. Lobosco. Computational modeling of the immune response to yellow fever. *J. Comput. Appl. Math.*, 295:127–138, 2016.

[3] C.R.B. Bonin, G.C. Fernandes, R.W. dos Santos, and M. Lobosco. A qualitatively validated mathematical-computational model of the immune response to the yellow fever vaccine. *BMC Immunol.*, 19(1):15, 2018.

[4] C.R.B. Bonin, G.C. Fernandes, R.M. Menezes, L.A.B. Camacho, L.M.H. da Mota, S.M.B. de Lima, A.C. Campi-Azevedo, O.A. Martins-Filho, R. W. dos Santos, M. Lobosco, et al. Quantitative validation of a yellow fever vaccine model. In *2019 IEEE International Conference on Bioinformatics and Biomedicine (BIBM)*, pages 2113–2120, 2019.

[5] R.L. Burden, J.D. Faires, and A.M. Burden. *Numerical Analysis*. Cengage Learning, 2015.

[6] M. Catanzaro, F. Fagiani, M. Racchi, E. Corsini, S. Govoni, and C. Lanni. Immune response in COVID-19: addressing a pharmacological challenge by targeting pathways triggered by SARS-CoV-2. *Sign. Transduct. Target. Ther.*, 5(1):1–10, 2020.

[7] S.T. Chang, J.J. Linderman, and D.E. Kirschner. Multiple mechanisms allow mycobacterium tuberculosis to continuously inhibit mhc class ii-mediated antigen presentation by macrophages. *Proc. Ntl. Acad. Sci. United States Amer.*, 102(12):4530–4535, 2005.

[8] D.L. Chao, M.L. Davenport, S. Forrest, and A.S. Perelson. A stochastic model of cytotoxic T cell responses. *J. Theoret. Biol.*, 228(2):227–240, 2004.

[9] G.G. Davanzo, A.C. Codo, N.S. Brunetti, et al. SARS-CoV-2 uses cd4 to infect t helper lymphocytes. *medRxiv*, 2020.

[10] B. de M. Quintela, R.W. dos Santos, and M. Lobosco. On the Coupling of Two Models of the Human Immune Response to an Antigen. *BioMed Res. Int.*, 2014:e410457, 2014.

[11] M. Ehrhardt and R.E. Mickens. *A Nonstandard Finite Difference Scheme for Solving a Zika Virus Model*. Unpublished manuscript, 2017.

[12] J. Feinberg and H.P. Langtangen. Chaospy: An open source tool for designing methods of uncertainty quantification. *J. Comput. Sci.*, 11:46–57, 2015.

[13] J.A. Flegg, H.M. Byrne, M.B. Flegg, and D.L.S. McElwain. Wound healing angiogenesis: the clinical implications of a simple mathematical model. *J. Theor. Bio.*, 300:309–316, 2012.

[14] S. Goutelle, M. Maurin, F. Rougier, X. Barbaut, L. Bourguignon, M. Ducher, and P. Maire. The Hill equation: a review of its capabilities in pharmacological modelling. *Fundam. Clin. Pharmacol.*, 22(6):633–648, Dec 2008.

[15] R.A. Grant, L. Morales-Nebreda, N.S. Markov, et al. Circuits between infected macrophages and T cells in SARS-CoV-2 pneumonia. *Nature*, 590(7847):635–641, 2021.

[16] M. Hoffmann, H. Kleine-Weber, S. Schroeder, et al. SARS-CoV-2 Cell Entry Depends on ACE2 and TMPRSS2 and Is Blocked by a Clinically Proven Protease Inhibitor. *Cell*, 181(2):271–280.e8, 2020.

[17] T. Homma and A. Saltelli. Importance measures in global sensitivity analysis of nonlinear models. *Reliability Engineering & System Safety*, 52(1):1–17, 1996.

[18] A.M. Jarrett, N.G. Cogan, and M.E. Shirtliff. Modelling the interaction between the host immune response, bacterial dynamics and inflammatory damage in comparison with immunomodulation and vaccination experiments. *Math. Med. Biol.*, 32(3):285–306, 2015.

[19] M.H. Maamar, M. Ehrhardt, and L. Tabharit. A nonstandard finite difference scheme for a time-fractional model of Zika virus transmission. *IMACM Preprint 22/21*, 2022.

[20] R.E. Mickens. *Applications of nonstandard finite difference schemes*. World Scientific, 2000.

[21] R.E. Mickens. Exact solutions to a finite-difference model of a nonlinear reaction-advection equation: Implications for numerical analysis. *J. Diff. Eqs. Appl.*, 9(11):313–325, 2003.
[22] K. Murphy and C. Weaver. *Janeway's immunobiology*. Garland Science, 2008.
[23] W.E. Paul. *Fundamental Immunology*. Fundamental Immunology. Wolters Kluwer/Lippincott Williams & Wilkins, 2008.
[24] A.S. Perelson. Modeling the interaction of the immune system with HIV. In *Mathematical and statistical approaches to AIDS epidemiology*, pages 350–370. Springer, 1989.
[25] G.J. Pettet, H.M. Byrne, D.L.S McElwain, and J. Norbury. A model of wound-healing angiogenesis in soft tissue. *Math. Biosci.*, 136(1):35–63, 1996.
[26] A. B. Pigozzo, D. Missiakas, S. Alonso, R. W. Dos Santos, and M. Lobosco. Development of a Computational Model of Abscess Formation. *Front Microbiol*, 9:1355, 2018.
[27] A.B. Pigozzo, G.C. Macedo, R.W. dos Santos, and M. Lobosco. On the computational modeling of the innate immune system. *BMC Bioinformatics*, 14(6):S7, 2013.
[28] K. Price, R.M. Storn, and J.A. Lampinen. *Differential evolution: a practical approach to global optimization*. Springer Science & Business Media, 2006.
[29] R. F. Reis, J. L. Fernandes, T. R. Schmal, B. M. Rocha, R. W. Dos Santos, and M. Lobosco. A personalized computational model of edema formation in myocarditis based on long-axis biventricular MRI images. *BMC Bioinformatics*, 20(Suppl 6):532, Dec 2019.
[30] R.F. Reis, A.B. Pigozzo, C.R.B. Bonin, B. Quintela, L.T. Pompei, A.C. Vieira, M.P. Xavier, R. Weber dos Santos, M. Lobosco, et al. A validated mathematical model of the cytokine release syndrome in severe COVID-19. *Front. Molecular Biosci.*, page 680, 2021.
[31] H. Ritchie, E. Mathieu, L. Rodés-Guirao, C. Appel, C. Giattino, E. Ortiz-Ospina, J. Hasell, B. Macdonald, D. Beltekian, and M. Roser. Coronavirus pandemic (COVID-19). *Our World in Data*, 2020. https://ourworldindata.org/coronavirus.
[32] A. Rohatgi. Webplotdigitizer: Version 4.3, 2020.
[33] Scipy. scipy.optimize.differential_evolution, accessed on December, 2022.
[34] Scipy. Scipy's homepage, accessed on December, 2022.
[35] J. Shang, Y. Wan, C. Luo, et al. Cell entry mechanisms of SARS-CoV-2. *Proc. Nat. Acad. Sci.*, 117(21):11727–11734, 2020.
[36] I.M. Sobol. On sensitivity estimation for nonlinear mathematical models. *Matematicheskoe Modelirovanie*, 2(1):112–118, 1990.
[37] I.M. Sobol. Global sensitivity indices for nonlinear mathematical models and their Monte Carlo estimates. *Math. Comput. Simul.*, 55(1-3):271–280, 2001.
[38] L. Sompayrac. *How the Immune System Works*. Wiley-Blackwell, Oxford, 2012.
[39] R. Storn and K. Price. Differential evolution – a simple and efficient heuristic for global optimization over continuous spaces. *J. Global Optim.*, 11(4):341–359, 1997.
[40] B. Su, W. Zhou, K.S. Dorman, and D.E. Jones. Mathematical modelling of immune response in tissues. *Comput. Math. Meth. Med.*, 10(1):9–38, 2009.
[41] K.K.-W. To, O.T.-Y. Tsang, W.-S. Leung, A.R. Tam, T.-C. Wu, D.C. Lung, C.C.-Y. Yip, J.-P. Cai, J.M.-C. Chan, T.S.-H. Chik, et al. Temporal profiles of viral load in posterior oropharyngeal saliva samples and serum antibody responses during infection by SARS-CoV-2: an observational cohort study. *The Lancet Infectious Diseases*, 20(5):565–574, 2020.
[42] Y. Vodovotz, C.C. Chow, J. Bartels, et al. In silico models of acute inflammation in animals. *Shock*, 26(3):235–244, 2006.
[43] World Health Organization. WHO Timeline - COVID-19 - 27 April 2020. `https://www.who.int/news/item/27-04-2020-who-timeline---covid-19`, 2020. Last accesses on October 22 of 2021.
[44] M.P. Xavier, C.R. Bonin, R.W. dos Santos, and M. Lobosco. On the use of Gillespie stochastic simulation algorithm in a model of the human immune system response to the Yellow Fever vaccine. In *2017 IEEE Int. Conf. on Bioinformatics and Biomedicine (BIBM)*, pages 1476–1482, 2017.
[45] C. Zhang, Z. Wu, J.-W. Li, H. Zhao, and G.-Q. Wang. Cytokine release syndrome in severe COVID-19: interleukin-6 receptor antagonist tocilizumab may be the key to reduce mortality. *Int. J. Antimicr. Agents*, 55(5):105954, 2020.
[46] X. Zhang, Y. Tan, Y. Ling, et al. Viral and host factors related to the clinical outcome of COVID-19. *Nature*, 583(7816):437–440, 2020.

Institute of Exact Sciences, Department of Computing, Federal University of Juiz de Fora, Juiz de Fora, Brazil

FISIOCOMP - Laboratory of Computational Fisiology and High-Performance Computing
Email address: gustavo.morais@estudante.ufjf.br

Department of Computer Science and Graduate Program in Computational Modeling, Federal University of Juiz de Fora, Juiz de Fora, Brazil

FISIOCOMP - Laboratory of Computational Fisiology and High-Performance Computing
Email address: marcelo.lobosco@ice.ufjf.br

Chair of Applied and Computational Mathematics, University of Wuppertal, Wuppertal, Germany
Email address: ehrhardt@uni-wuppertal.de

Department of Computer Science and Graduate Program in Computational Modeling, Federal University of Juiz de Fora, Juiz de Fora, Brazil

FISIOCOMP - Laboratory of Computational Fisiology and High-Performance Computing
Email address: ruy.reis@ufjf.br